Neurobiology of Aging 34 (2013) 2574–2584

Contents lists available at SciVerse ScienceDirect

Neurobiology of Aging

journal homepage: www.elsevier.com/locate/neuaging

Cannabinoid receptor 1 deficiency in a mouse model of Alzheimer's disease leads to enhanced cognitive impairment despite of a reduction in amyloid deposition

Christoph Stumm [a,1], Christof Hiebel [a,1], Regina Hanstein [a,2], Martin Purrio [b], Heike Nagel [a], Andrea Conrad [b], Beat Lutz [b], Christian Behl [a,*], Angela B. Clement [a,**]

[a] Institute for Pathobiochemistry, University Medical Center, Johannes Gutenberg University Mainz, Mainz, Germany
[b] Institute for Physiological Chemistry, University Medical Center, Johannes Gutenberg University Mainz, Mainz, Germany

ARTICLE INFO

Article history:
Received 26 November 2012
Received in revised form 18 May 2013
Accepted 27 May 2013
Available online 6 July 2013

Keywords:
Alzheimer's disease
Endocannbinoid system
CB1
APP processing
APP23
Learning and memory

ABSTRACT

Alzheimer's disease (AD) is characterized by amyloid-β deposition in amyloid plaques, neurofibrillary tangles, inflammation, neuronal loss, and cognitive deficits. Cannabinoids display neuromodulatory and neuroprotective effects and affect memory acquisition. Here, we studied the impact of cannabinoid receptor type 1 (CB1) deficiency on the development of AD pathology by breeding amyloid precursor protein (APP) Swedish mutant mice (APP23), an AD animal model, with CB1-deficient mice. In addition to the lower body weight of APP23/CB1$^{-/-}$ mice, most of these mice died at an age before typical AD-associated changes become apparent. The surviving mice showed a reduced amount of APP and its fragments suggesting a regulatory influence of CB1 on APP processing, which was confirmed by modulating CB1 expression in vitro. Reduced APP levels were accompanied by a reduced plaque load and less inflammation in APP23/CB1$^{-/-}$ mice. Nevertheless, compared to APP23 mice with an intact CB1, APP23/CB1$^{-/-}$ mice showed impaired learning and memory deficits. These data argue against a direct correlation of amyloid plaque load with cognitive abilities in this AD mouse model lacking CB1. Furthermore, the findings indicate that CB1 deficiency can worsen AD-related cognitive deficits and support a potential role of CB1 as a pharmacologic target.

1. Introduction

Alzheimer's disease (AD) is the major neurodegenerative disease in humans. Clinically, cognitive deficits of AD patients correlate with cerebral atrophy in vulnerable brain regions, mainly in the frontal cortex and the hippocampal region. Pathologically, AD involves neurofibrillary degeneration and the progressive deposition of self-aggregating amyloid-β (Aβ) peptides in extracellular amyloid plaques that are surrounded by activated astrocytes and microglia (Johnston et al., 2011; Schellenberg and Montine, 2012). A major focus of AD research lies on the development of therapeutic strategies that block processing of amyloid precursor protein (APP) to Aβ peptides. Aβ is generated by the subsequent cleavage of APP by β- and γ-secretase. Cleavage of APP by β-secretase can be inhibited by stimulation of α-secretase that cleaves APP in the Aβ domain, thus preventing Aβ release (Haass and Selkoe, 2007; Huang and Mucke, 2012). Stimulation of α-secretase activity has shown neuroprotective effects (Postina et al., 2004). Besides the decrease of Aβ production and aggregation, attenuation of the AD-associated neuroinflammation and reduction of neuronal damage caused by oxidative stress are further important therapeutical strategies.

The neuroprotective effects of cannabinoids have been studied in a variety of neurodegenerative paradigms, and our understanding concerning the influence of cannabinoids on AD pathology is growing (Aso et al., 2012; Bisogno and Di Marzo, 2008; Esposito et al., 2011; Iuvone et al., 2009; Karl et al., 2012). Brains of AD patients show a strong overexpression of CB2 in activated microglia and of fatty acid amide hydrolase in activated astrocytes (Benito et al., 2003). A previous report showed a decreased number of cannabinoid receptor type 1 (CB1)–positive neurons in the frontal cortex of brains of AD patients in areas with amyloid plaques and activated microglial cells (Ramirez et al., 2005). This reduction of CB1-positive neurons is accompanied by an alteration of the expression and cellular localization of endocannabinoid

* Corresponding author at: Institute for Pathobiochemistry, University Medical Center, Johannes Gutenberg University Mainz, Duesbergweg 6, 55099 Mainz, Germany. Telephone: +49 (0)6131 39 25890 Fax.: +49 (0)6131 39 25792
** Alternate corresponding author at: Institute for Pathobiochemistry, University Medical Center, Johannes Gutenberg University Mainz, Duesbergweg 6, 55099 Mainz, Germany.
E-mail addresses: cbehl@uni-mainz.de (C. Behl), clemena@uni-mainz.de (Angela B. Clement).
[1] These two authors contributed equally to this study.
[2] Present address: Department of Neuroscience, Albert Einstein College of Medicine, Bronx, NY 10461, USA.

0197-4580/$ – see front matter © 2013 Elsevier Inc. All rights reserved.
http://dx.doi.org/10.1016/j.neurobiolaging.2013.05.027

synthesizing and degrading enzymes (diacylglycerol lipase and monoacylglycerol lipase) in brains of AD patients (Mulder et al., 2011). In addition, in vivo and in vitro data suggested that cannabinoid receptor agonists can protect neurons against amyloid-induced toxicity (Martin-Moreno et al., 2011, 2012; Ramirez et al., 2005). Moreover, it was also shown that AD-associated Aβ peptides influence endocannabinoid signaling, and there is an interplay between endocannabinoid signaling and Aβ toxicity (Chen et al., 2011; Jung et al., 2012; Mazzola et al., 2003; Mulder et al., 2011; van der Stelt et al., 2006). Specifically, intracerebroventricular coadministration of the mixed synthetic CB1 and CB1 agonist Win55,212-2 with a toxic Aβ peptide to rats prevented Aβ-induced microglial activation, cognitive impairment, and neuronal loss. This study was extended by in vitro experiments disclosing inhibition of Aβ-induced microglial activation by CB1 and CB2 agonists and neuroprotective effects on primary rat neurons. Prolonged oral cannabinoid administration to TgAPP2576 mice also showed beneficial effects, such as a reduced inflammation, a lower cortical accumulation of Aβ peptides, and an improved cortical performance (Martin-Moreno et al., 2012). Several mechanisms by which cannabinoids might exert their neuroprotective and anti-inflammatory effects, such as the involvement of mitogen-activated protein kinases and glycogen synthase kinase 3-beta signaling pathways (Martin-Moreno et al., 2012; Milton, 2002), the inhibition of acetylcholinesterase activity and acetylcholinesterase-induced Aβ aggregation (Eubanks et al., 2006), and antioxidant properties (Marsicano et al., 2002a), have been proposed. The neuroprotective and anti-inflammatory activities of Win55,212-2 against Aβ-induced damage in rats were recently shown to be mediated by CB1 and CB2 (Fakhfouri et al., 2012). Recently, CB1 was found to be expressed in mitochondria, and a novel role for CB1 receptors in the regulation of energy metabolism in the brain was proposed (Benard et al., 2012). Because the energy demand of the brain is rather high, a dysfunction of mitochondrial CB1 or a deficiency could have significant consequences for neuronal function and survival. Collectively, these data indicate that cannabinoid receptors may be promising therapeutic targets in AD.

The described changes in the endocannabinoid signaling system in brains of AD patients and the observed beneficial effects after cannabinoid administration in vitro and in vivo prompted us to generate a novel mouse model by knocking out CB1 expression in APP23 mice, a recognized AD mouse model, to study the impact of CB1 deficiency on the development of AD pathology.

2. Materials and methods

2.1. Reagents

Unless stated otherwise, all reagents were from regular commercial sources. All used antibodies and their sources are described in Table 1.

2.2. Cell culture

Mouse N2A neuroblastoma cells (provided by Claus Pietrzik, University Medical Center Mainz) were cultured in Dulbecco's Modified Eagle's Medium, 1 mM Minimum Essential Medium Sodium Pyruvate (both Gibco) supplemented with antibiotics and antimycotics (Invitrogen, Karlsruhe, Germany), and 10% active fetal calf serum (PAA, Pasching, Austria). N2A cells were transfected with 10 μg peGFPN1 (Clontech, Mountain View, CA USA), pcDNA3-human CB1 (Missouri S&T cDNA Resource Center, Rolla, MO, USA), or peGFPN1-mouse CB1 (Dodd et al., 2010) in electroporation buffer (135 mM KCl, 0.2 mM $CaCl_2$, 2 mM $MgCl_2$, 10 mM HEPES, 5 mM EGTA, 25% heat-inactivated fetal calf serum [pH 7.3]; modified from Buchser et al., 2006) using an Amaxa electroporation system according to the manufacturer's instructions (Amaxa, Cologne, Germany; program T-24). Stably transfected cells were selected using 1 mg/mL G418 (PAA) as selection antibiotics and subcloned by limited dilution. For analyzing the effect of CB1 expression on APP processing, cells were seeded at 10,000 cells/cm^2 on a 60-cm^2 cell culture dish in 10 mL medium. Medium was changed once after 24 hours. After 48 hours, medium was collected and cleared from cells and cell debris by centrifugation (3000 *g*, 4 °C for 5 minutes). Cells were washed once with ice-cold phosphate-buffered saline (PBS) (Invitrogen, Karlsruhe, Germany) and scraped into ice-cold PBS. Cells were pelleted by centrifugation (3000 *g*, 4 °C for 5 minutes) and resuspended in 100 μL of 50 mM Tris-Cl, 10% sucrose, 1 mM EDTA, 1 mM EGTA, 15 mM HEPES, 1 mM sodium orthovanadate, 1 mM sodium fluoride, phosphatase inhibitor cocktail (Phos-Stop; Roche, Basel, Switzerland), and proteinase cocktail (complete EDTA-free; Roche). Cells were disrupted by sonication using a tip sonicator. Protein concentration was determined using a BCA kit (Pierce) with bovine serum albumin as a standard. Thirty micrograms of the total cell lysate per lane and 45 μL medium per lane were subjected to sodium dodecyl sulfate (SDS)-polyacrylamide gel electrophoresis on 10%–15% Bis-Tris gradient gels and analyzed by Western blotting using the appropriate antibodies as stated in Section 3.

For CB1-knockdown studies, subconfluent cells of a 20-cm^2 dish were transfected with 20 μg double-stranded small interfering RNA (siRNA) as described previously. siRNA was designed by MWG Biotech (Ebersberg, Germany) and used for transfection after dilution at 1 μg/mL in 1× Universal buffer (MWG Biotech). siRNA sequences (sense strand) are given in Table 2. Cells were used for experiments 48 hours after transfection. CB1 and APP messenger RNA (mRNA) levels were assessed after each experiment by quantitative real-time polymerase chain reaction (qPCR). Level of housekeeping gene *ribosomal protein L19* mRNA (RPL19) served as an internal control. The primers used for reverse transcriptase (RT)-PCR and qPCR analyses are given in Table 2.

Table 1
Antibodies

Antibodies	Species	Dilution	Supplier
Primary antibodies for immunohistochemistry			
Anti-Aβ1-16 (6E10)	Mouse	1:100	Covance
Anti-GFAP	Rabbit	1:100	Dako
Anti-Iba1	Rabbit	1:100	Wako
Anti-NeuN	Mouse	1:100	Chemicon
Anti-synaptophysin 1	Rat	1:200	Synaptic Systems
Primary antibodies for immunoblots			
Actin	Rabbit	1:1000	Sigma
CB1	Rabbit	1:200	Cayman Chemical
Anti-Aβ1–16 (6E10)	Mouse	1:1000	Covance
$APP_{C\text{-terminus}}$ (A8717)	Rabbit	1:1000	Sigma
$APP_{N\text{-terminus}}$ (22C11)	Mouse	1:1000	Chemicon
Anti-GFAP	Rabbit	1:1000	Dako
Anti-NeuN	Mouse	1:1000	Chemicon
Anti-synaptophysin 1	Mouse	1:1000	Synaptic Systems
Anti-PSD95	Mouse	1:1000	J. Trotter, Mainz
Secondary antibodies for immunohistochemistry			
AlexaFluor647-anti-rabbit	Goat	1:200	Jackson
Cy3-anti-mouse	Goat	1:200	Jackson
Cy3-anti-rat	Goat	1:200	Jackson
Cy2-anti-mouse	Goat	1:200	Jackson
Secondary antibodies for immunoblots			
Anti-mouse-HRP	Donkey	1:10,000	Jackson
Anti-rabbit-HRP	Donkey	1:10,000	Jackson
Anti-rat-HRP	Donkey	1:10,000	Jackson

Key: GFAP, glial fibrillary acidic protein; HRP, horse radish peroxidase; PSD95, postsynaptic density protein 95.

Table 2
siRNA and primer sequences used for RT-PCR and qPCR analyses

siRNA sequences	
Nonsense siRNA	5′-GGGAAAUGCGUUAGCAGUGAU-3′
Mouse CB1 siRNA -1	5′-AGAUGACGGCAGGAGACAA-3′
Mouse CB1 siRNA -2	5′-CCAACAUUACAGAGUUCUA-3′
Primers used in RT-PCR and qPCR analyses	
Human/mouse RPL19 for	5′-GAAATCGCCAATGCCAACTC-3′
Human/mouse RPL19 rev	5′-TTCCTTGGTCTTAGACCTGCG-3′
Human CB1 forward	5′-CGTCTGAGGATGGGAAGGTA-3′
Human CB1 reverse	5′-TGTCGCAGGTCCTTACTCCT-3′
Mouse CB1 forward	5′-GTCACCAGTGTGCTGTTGCT-3′
Mouse CB1 reverse	5′-TCAACACCACCAGGATCAGA-3′
Mouse APP forward	5′-GGAAGCAGCCAATGAGAGAC-3′
Mouse APP reverse	5′-GTTCATGCGCTCGTAGATCA-3′
Primers used for mouse genotyping	
cnr1-KO 5′(loxP)	5′-GCTGTCTCTGGTCCTCTTAAA-3′
cnr1-KO 3′(loxP)	5′-GGTGTCACCTCTGAAAACAGA-3′
cnr1-KO neo-0 3′	5′-CCTACCCGGTAGAATTAGCTT-3′
APP23 forward	5′-GAATTCCGACATGACTCAGG-3′
APP23 reverse	5′-GTTCTGCTGCATCTTGGACA-3′
Actin forward	5′-GACAGGATGCAGAAGAGAAT-3′
Actin reverse	5′-TTGCTGATCCACATCTGCTG-3′

Key: APP, amyloid precursor protein; CB1, cannabinoid receptor type 1; RPL19, ribosomal protein L19; RT-PCR, reverse-transcriptase polymerase chain reaction; siRNA, small interfering RNA; qPCR, quantitative real-time PCR.

2.3. RT-PCR and qPCR analyses

Total RNA from subconfluent cell cultures was extracted using the Absolutely RNA Mini kit according to the manufacturer's instructions (Agilent, Böblingen, Germany). Reverse transcription was performed on 500 ng total RNA in a final reaction volume of 20 μL containing 2 μL RT buffer (Qiagen, Hilden, Germany), 2 μL deoxyribonucleotide triphosphates (5 mM; Qiagen), 2 μL oligo(dT)15 primer (10 μM; Promega, Mannheim, Germany), 10 U RNasin (Promega), and 4 U Omniscript Reverse Transcriptase (Qiagen). Synthesis of complementary DNA (cDNA) was carried out for 60 minutes at 37 °C. PCR was performed in a 25-μL reaction volume containing 2 μL cDNA, 2.5 μL 10× PCR buffer (Invitrogen), 0.75 μL $MgCl_2$ (50 mM; Invitrogen), 0.5 μL deoxyribonucleotide triphosphates (10 mM; PeqLAB), 0.5 U DNA Taq Polymerase (Invitrogen), and 0.5 μL of sense and antisense primers (100 pmol; MWG-Biotech AG). After 3 minutes of initial denaturation at 95 °C, PCR conditions were 95 °C for 1 minute, 60 °C for 20 seconds, and 72 °C for 30 seconds for 35 cycles.

For relative quantification of mRNA, qPCR was performed in a 25-μL reaction volume containing 1 μL cDNA, 0.5 μL forward and reverse primers (100 pmol), 12.5 μL of 2× Absolute qPCR SYBR Green Mix (Thermo Scientific), and 10.5 μL water using the iCycler real-time thermocycler (Bio-Rad). After 15 minutes of initial denaturation at 95 °C, PCR conditions were 95 °C for 30 seconds, 60 °C for 30 seconds, and 72 °C for 30 seconds for 35 cycles. The first PCR cycle that generated a fluorescence signal above the threshold (Ct) was determined. The confirmation of PCR product specificity was done by analysis of the melting curves of each PCR product. Relative gene expression was calculated using the relative expression software tool (REST, Pfaffl et al., 2002). Ribosomal protein L19 (RPL19) gene was used as a reference gene for all experiments. Primer sequences used for RT-PCR and qPCR analyses are listed in Table 2.

2.4. Animals

We generated mice with a hemizygous expression of the AD-linked KM670/671NL double mutation (Swedish mutation) of human APP under the control of a neuron-specific Thy-1 promoter

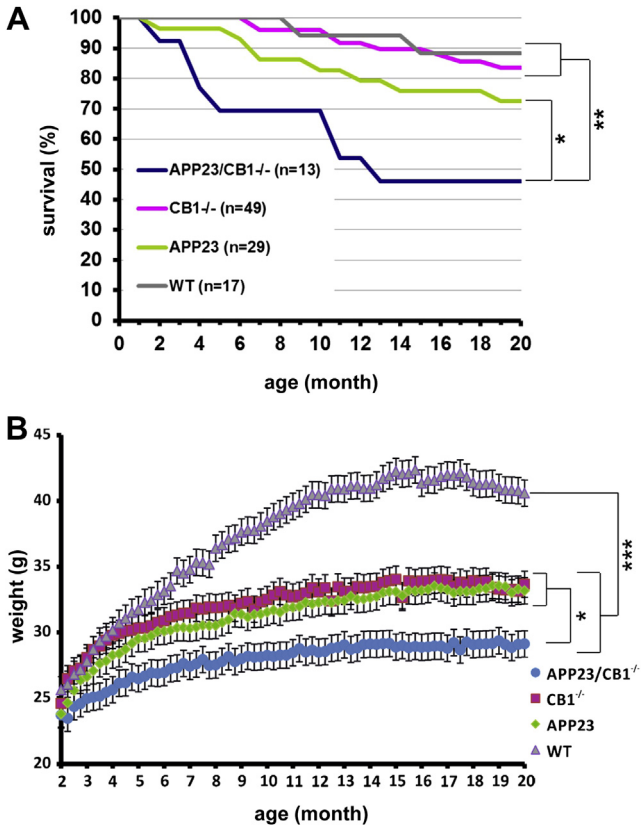

Fig. 1. Cannabinoid receptor type 1 (CB1) deletion in APP23 mice results in reduced survival and body weight. (A) Survival curve of all genotypes over 20 months. The number of animals is indicated. Statistical analysis was performed using the Breslow test ** $p < 0.01$ for APP23/CB1$^{-/-}$ compared with CB1$^{-/-}$ and wild-type (WT) and * $p < 0.05$ compared with APP23. (B) Weight curve of all genotypes over 20 months. Shown are mean ± standard error of the mean. Weight data were analyzed by repeated-measures 2-way analysis of variance (Fisher least significant difference) from 3 to 20 months of age (APP23/CB1$^{-/-}$ [n = 7], CB1$^{-/-}$ [n = 9], APP23 [n = 12], and WT [n = 11] mice; *** $p < 0.005$, * $p < 0.05$).

fragment in a CB1$^{+/+}$ (here labeled as APP23) or a CB1$^{-/-}$ (APP23/CB1$^{-/-}$) background. APP23 mice (always bred and analyzed in hemizygosity: APP$^{swe/wt}$) and CB1$^{-/-}$ mice have been generated previously (Marsicano et al., 2002b; Sturchler-Pierrat et al., 1997). Both strains are kept on a C57BL6n background. APP23 mice were crossed with CB1$^{+/-}$ mice. Animals from the resulting F1 generation were crossed to obtain APP23/CB1$^{-/-}$ mice and their control littermates. After initially crossing CB1$^{+/-}$ × APP23/CB1$^{+/-}$ (n = 11), we counted a smaller number of APP23/CB1$^{-/-}$ mice after genotyping (at an age of about 6 weeks) than expected according to Mendelian laws. In fact, because we only used male animals for our experiments, the number of animals was too small to set up meaningful experiments. Therefore, we in addition crossed CB1$^{-/-}$ × APP23/CB1$^{+/-}$ (n = 12), which also resulted in a smaller number of APP23/CB1$^{-/-}$ mice than expected according to Mendelian laws and had the disadvantage that not all necessary control genotypes can be obtained by this breeding strategy. The missing control genotypes were obtained by crossing APP23/CB1$^{+/-}$ × wild type (WT, n = 3). Mice from all 3 breeding strategies were used for the experiments. Mice were genotyped by PCR using primers described in Table 2. All mice were single housed at least 7 days before experiments on a 12:12 hour light-dark schedule with food and water available ad libitum. Animal procedures were performed according to the guidelines of the European Communities Council Directive of November 24, 1986 (86/609/EEC) and the German

Council on Animal Care. The experimental design was made to minimize animal suffering and number of animals. For our experiments, only male mice were used. Survival was estimated over 20 months. Body weight was determined weekly over 20 months.

2.5. Western blotting

Mice were sacrificed, brains were removed, and the hippocampal region of the left hemisphere was immediately snap frozen in liquid nitrogen. Tissue samples were dounced in ice-cold 20 mM Tris-Cl, pH 6.8, supplemented with protease- and phosphatase-inhibitor cocktails (Roche), and then centrifuged at 100,000 *g* for 45 minutes at 4 °C to separate soluble from membrane-bound proteins. The soluble fraction was stored on ice until further use. The membrane fraction was resuspended in 85 mM Tris-Cl, pH 6.8, 3% sodium dodecyl sulfate, and 5% sucrose plus protease- and phosphatase-inhibitor cocktail and sonicated with a tip sonicator 3 times for 10 seconds. Protein concentration was determined using a BCA kit (Pierce) with bovine serum albumin as a standard. Thirty micrograms of protein per lane from the soluble or membrane fractions were separated by SDS-polyacrylamide gel electrophoresis on 4%–12% Bis-Tris gradient gels (Invitrogen) and analyzed by Western blotting with the appropriate antibodies. Western blot signals were quantified by AIDA Image software. Actin or Coomassie staining of an SDS gel run in parallel was used to ensure equal protein loading.

2.6. Aβ enzyme-linked immunosorbent assay

$A\beta_{1-40}$ and $A\beta_{1-42}$ levels in soluble fractions of hippocampal extracts were measured by enzyme-linked immunosorbent assay (ELISA) kits (Merck, Darmstadt, Germany) following the manufacturer's instructions.

2.7. Histochemistry

Immediately after preparation, the right brain hemispheres were submersed into 4% paraformaldehyde for 24 hours at 4 °C for

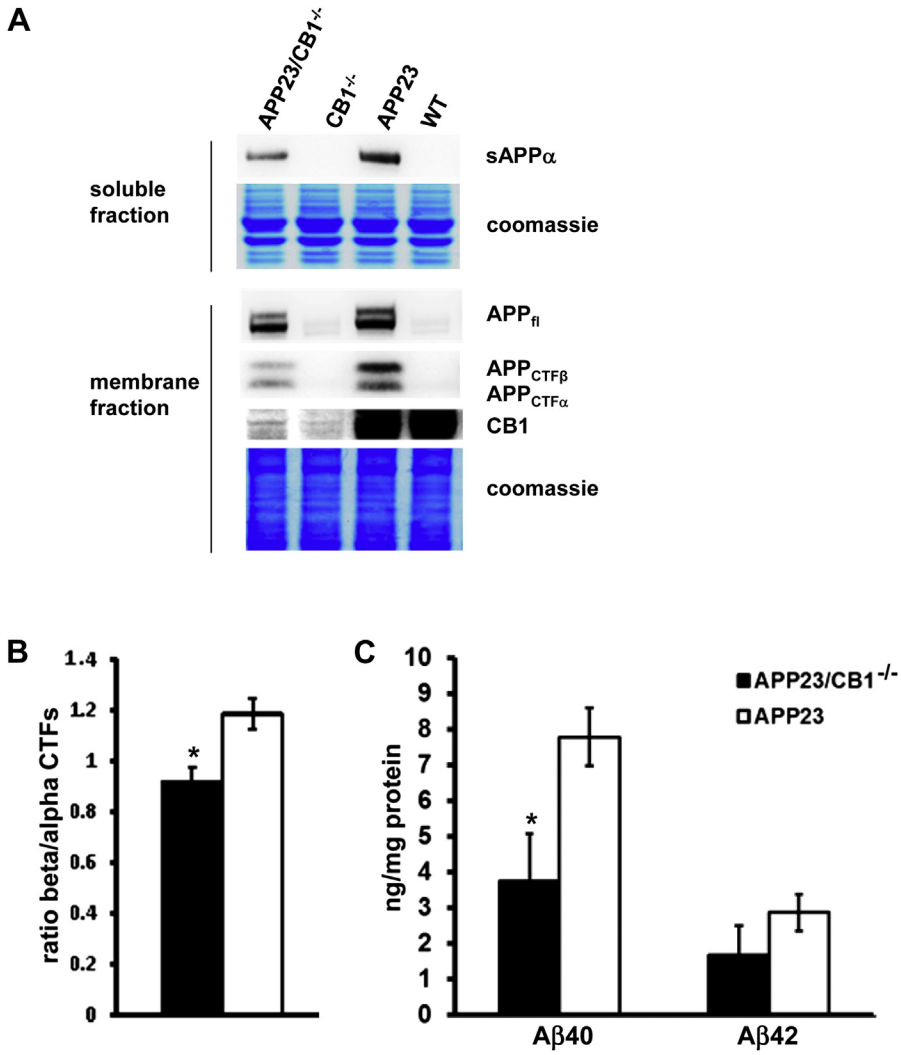

Fig. 2. Cannabinoid receptor type 1 (CB1) control expression and processing of mutant amyloid precursor protein (APP) in the Alzheimer's disease mouse model. (A) Expression of mutant APP, its secreted $sAPP_{\alpha}$ fragment, and the membrane-bound C-terminal α and β fragments (CTF_{α} and CTF_{β}) as determined by Western blot analysis of differentially processed hippocampal extracts of 20-month-old mice (n = 4 for APP23/$CB1^{-/-}$, n = 7 for other genotypes). Coomassie staining of sodium dodecyl sulfate gels run in parallel was used to ensure equal protein loading. (B) Quantification of CTF_{β} to CTF_{α} ratio as obtained by Western blot analysis of differentially processed hippocampal extracts of 20-month-old mice (n = 5 for APP23/$CB1^{-/-}$, n = 10 for APP23). (C) The amount of amyloid β ($A\beta$)$_{40}$ and $A\beta_{42}$ peptides was determined by Aβ peptide–specific enzyme-linked immunosorbent assay and is shown as mean ± standard error of the mean. * $p < 0.05$ compared with APP23 (Students *t* test) in (B) and (C).

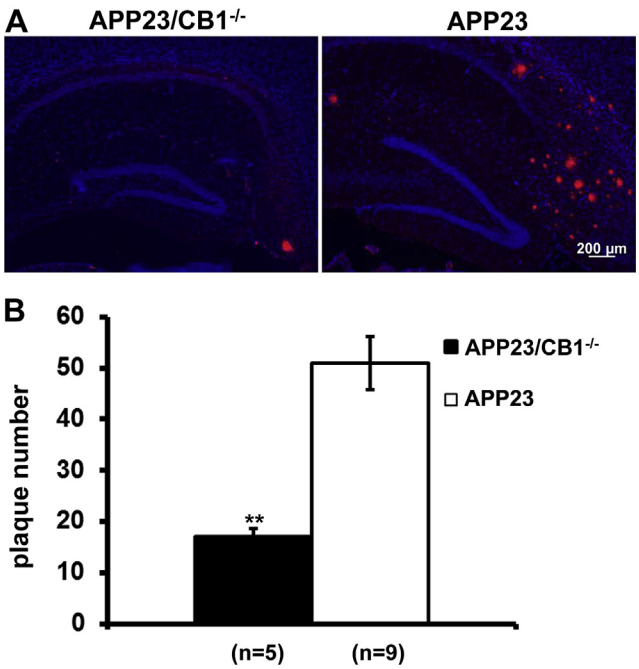

Fig. 3. Cannabinoid receptor type 1 (CB1) depletion in APP23 mice and amyloid plaque load. (A) Numerous plaques were found in brains of 20-month-old APP23 mice by immunofluorescence staining with amyloid β antibody 6E10. (B) The number of amyloid plaques was significantly reduced in the cortices and hippocampi of APP23/CB1$^{-/-}$ (n = 5) mice compared with APP23 mice (n = 9). The average number of plaques was determined in 3 brain sections per animal located between −2.70 and −1.70 mm to bregma. Shown are the means ± standard error of the mean. Bar = 200 µm. ** $p < 0.01$ (Student t test).

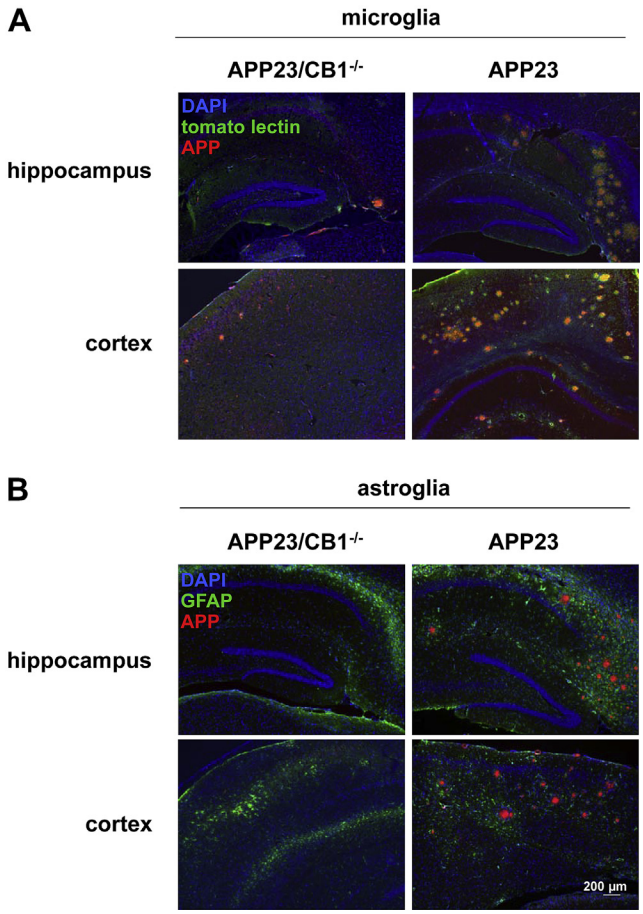

Fig. 4. Extent of glial inflammation mirrors amyloid plaque load. Amyloid plaques were stained with the monoclonal antibody 6E10 (red), which binds within the amyloid β region of amyloid precursor protein (APP). Glial inflammation was visualized (green) by staining of activated microglial cells with fluorescein isothiocyanate–coupled tomato lectin (A) and of activated astroglial cells with glial fibrillary acidic protein (GFAP) antibody (B). Nuclei were counterstained with 4′-6-diamidino-2-phenylindole dihydrochloride (DAPI) (blue). Bar = 200 µm (n = 3 for each genotype).

fixation and subsequently incubated for 48 hours in 30% sucrose in PBS for cryoprotection. Then, the hemispheres were embedded in tissue freezing medium (Jung) in a dry ice - ethanol bath and cut into 10-µm-thick coronal sections. For immunohistochemistry, sections were postfixed for 20 minutes with 4% paraformaldehyde, subsequently incubated with 3% bovine serum albumin in 0.1% TritonX-100 in PBS at room temperature for permeabilization and blocking of unspecific binding sites, and then incubated overnight at 4 °C with the primary antibodies diluted in 0.1% TritonX-100 in PBS. Signals of primary antibodies were detected by incubation with Cy2- or Cy3-coupled secondary antibodies in 0.1% TritonX-100 in PBS for 1 hour at room temperature. Amyloid plaques were detected by immunohistochemistry using the monoclonal anti-APP antibody 6E10. Neurons were labeled by a monoclonal anti-NeuN antibody. Inflammation was monitored by estimating the level of the astrocytic marker protein, glial fibrillary acidic protein (GFAP), which is upregulated by activated astrocytes (Brahmachari et al., 2006) using a polyclonal anti-GFAP antibody and by fluorescein isothiocyanate–coupled tomato lectin (Sigma) or a polyclonal anti-Iba1 antibody, which detects microglial cells (Asuni et al., 2010; Persson et al., 2013). Counterstaining of nuclei was performed by addition of 0.5 µg/mL 4′-6-diamidino-2-phenylindole dihydrochloride (DAPI, Sigma) to the secondary antibody or tomato lectin solution. Stained sections were analyzed using an Axiovert 200 microscope (Zeiss). Quantification of amyloid plaque load was performed in a blinded manner by manually counting 6E10-antibody–labeled amyloid plaques in 3 sections per animal located between −2.70 and −1.70 mm to bregma and estimating the average number of plaques per animal. For estimating the degree of astroglial activation, 3 GFAP-stained sections per animal were photographed at a 40-fold magnification using fixed camera settings and the mean gray value per slice area was measured using the ImageJ program. The number of animals analyzed for each genotype is given in the figure legends. Confocal laser scanning microscopy was performed using an LSM 710 microscope (Zeiss).

2.8. Morris water maze test

Spatial learning and memory were investigated by the Morris water maze hidden platform task (Morris et al., 1982; Schmitt et al., 2006). The open-field circular water maze tank (97.1 cm in diameter, colored white) was filled with water (23 °C). Prominent objects around the maze provided spatial guidance cues. The task of the mouse was to escape from the water by locating a hidden escape platform (10 cm in diameter) submerged approximately 1.5 cm below the surface of the water. Before the first training trial, mice were set into the water for 3 minutes to get accustomed to the water. Mice performed 4 training trials per day (1 session) for 4 days with a maximum length of 60 seconds and an intertrial interval of 2 minutes under an infrared lamp to warm up and recreate. The platform made of clear perspex stayed in the same quadrant for all trials, and the animals were released from 4 different positions on the pool perimeter. The order was chosen randomly, and attention was paid that no sequence was repeated. Mice were allowed to stay for 30 seconds on the platform. Mice that did not find the platform within 60 seconds during training trials were guided to the

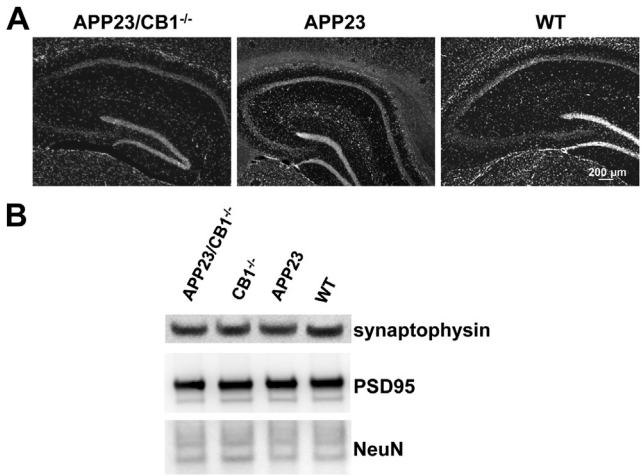

Fig. 5. (A) The hippocampal pyramidal cell layer of APP23 (n = 5) and APP23/CB1$^{-/-}$ mice (n = 4) showed no significant cell loss (thinning of CA1 region) compared with wild-type (WT) mice (n = 4) as revealed by 4′-6-diamidino-2-phenylindole dihydrochloride (DAPI) staining. (B) Western blot analysis of membrane extracts of the hippocampal region of 20-month-old mice showed similar expression of the neuron marker, NeuN, and of synaptic proteins, synaptophysin and postsynaptic density protein 95 (PSD95), in all genotypes (n = 3 for each genotype). Abbreviation: CB1, cannabinoid receptor type 1.

platform by the experimenter for 30 seconds to learn the position of the platform. During swimming, the swim paths were recorded by a CCD video camera mounted above the center of the tank. A computerized system registered the time to find the platform (escape latency) automatically. On the fifth day, a probe trial (60 seconds) without platform was performed. For the probe trial, the mice were set into the tank from a random position. For characterization of memory performance in the probe trial, the number of target crossings (target = former platform position) and time to reach the former platform location were recorded. The hardware consisted of an IBM-type AT computer combined with a video digitizer and a CCD video camera. Data acquisition and analysis were performed using Smart software (Panlab, Barcelona, Spain).

2.9. Statistical analysis

Data are presented as mean ± standard error of the mean. Water maze and weight data were analyzed by repeated-measures 2-way analysis of variance using SPSS software (IBM). Survival data were analyzed by the Breslow test using SPSS software. All other data were analyzed by Student *t* test using Sigma Stat software (SPSS Science). Differences were considered statistically significant if * $p < 0.05$, ** $p < 0.01$, or *** $p < 0.005$.

3. Results

3.1. Reduced survival and body weight of APP23/CB1$^{-/-}$ mice

APP23/CB1$^{-/-}$ mice showed a higher mortality rate than APP23, CB1$^{-/-}$, and WT mice, whereby about 50% of the deaths occurred during the first 5 months (Fig. 1A). Mice died suddenly, and postmortem autoptical analysis of dead animals revealed no obvious signs of pathologic changes. Furthermore, APP23/CB1$^{-/-}$ mice had a significantly lower body weight than APP23, CB1$^{-/-}$, and WT mice (Fig. 1B). APP23 and CB1$^{-/-}$ mice also showed a reduced body weight compared with WT mice that is not unexpected considering the described lean phenotype of CB1$^{-/-}$ mice (Cota et al., 2003) and the known weight loss of APP23 mice (Lalonde et al., 2005). Thus, regarding the body weight of the animals, the APP mutation and the knockout of CB1 appear to have additive effects. No other differences among genotypes were observed in general appearance or overt behavior.

3.2. Altered APP processing in brains of APP23/CB1$^{-/-}$ mice

The membrane fraction of hippocampal extracts of 20-month-old mice was analyzed by Western blot. With the anti-APP$_{C\text{-terminus}}$ antibody A8717, a reduction of the amount of full-length mutant APP (APP$_{fl}$) and its C-terminal α and β fragments (CTF$_\alpha$ and CTF$_\beta$) was observed in APP23/CB1$^{-/-}$ mice compared with APP23 mice (Fig. 2A). In addition, we found a strong decrease in levels of secreted sAPP$_\alpha$ (by Western blot analysis of the soluble fraction of hippocampal extracts using 6E10 antibody) and of Aβ_{1-40} peptide (by Aβ peptide–specific ELISA of the soluble fractions) in APP23/CB1$^{-/-}$ mice compared with APP23 mice (Figs. 2A and C). ELISA showed also a trend in the reduction of the Aβ_{1-42} peptide in APP23/CB1$^{-/-}$ mice compared with APP23 mice, although the observed difference was not statistically significant that could be because of sensitivity limitations of the ELISA to detect the Aβ_{1-42} peptide. Interestingly, we observed a shift from CTF$_\beta$ to CTF$_\alpha$, suggesting changes in intracellular APP localization and/or altered activities of APP-processing enzymes (Figs. 2A and B). A decrease in the amount of secreted sAPP$_\alpha$, APP$_{fl}$ protein, and the C-terminal APP fragments was already observed in 2-month-old APP23/CB1$^{-/-}$ animals, although the shift from CTF$_\beta$ to CTF$_\alpha$ was not yet observed at this age (Supplementary Fig. 1).

3.3. Reduced amyloid plaque load in APP23/CB1$^{-/-}$ mice

At the age of 14 months, first amyloid plaques in APP23 mice were detected by Congo Red and Aβ (6E10 antibody) staining (data not shown). In 20-month-old APP23 animals, numerous plaques were found in the cerebral cortex and in the hippocampal area (Fig. 3A), confirming the original observations in the first description of the APP23 mouse model (Sturchler-Pierrat et al., 1997). In the hippocampus, most plaques were found in the subiculum. Sporadically, plaques were detected in the CA1 region. The plaque number was significantly reduced in APP23/CB1$^{-/-}$ compared with the APP23 mice (Fig. 3B). Thus, the reduced amyloid plaque number in the APP23 mice with the CB1 deficiency is fully consistent with the observed reduced amount of Aβ peptides in these animals as detected by ELISA (Fig. 2C).

3.4. Analysis of hippocampal tissue: reduced glial inflammation in APP23/CB1$^{-/-}$ mice

APP23 mice are characterized by an extensive glial activation in close vicinity to amyloid plaques in the neocortex (Sturchler-Pierrat et al., 1997), which was confirmed in our analysis for the hippocampus as well using GFAP-antibody staining to detect astrogliosis and tomato lectin staining to label microglial cells. Overall, the extent of GFAP and tomato lectin staining was fully reflecting the amyloid plaque load of the brains (Fig. 3A) and was significantly lower in APP23/CB1$^{-/-}$ mice compared with APP23 mice as shown with GFAP staining (Fig. 4, Supplementary Figs. 2 and 4B). Whereas localization of activated microglial cells as detected by tomato lectin and IbaI staining was restricted to the close proximity of amyloid plaques in APP23 mice (Fig. 4A, Supplementary Figs. 3 and 4A), activated astrocytes as detected by GFAP staining were spread over a larger area but still surrounding the amyloid plaques in situ (Fig. 4B, Supplementary Fig. 4B).

We observed displacement of neurons adjacent to amyloid plaques in the cortex and hippocampus of all 20-month-old APP-overexpressing genotypes (shown for the neocortex of APP23

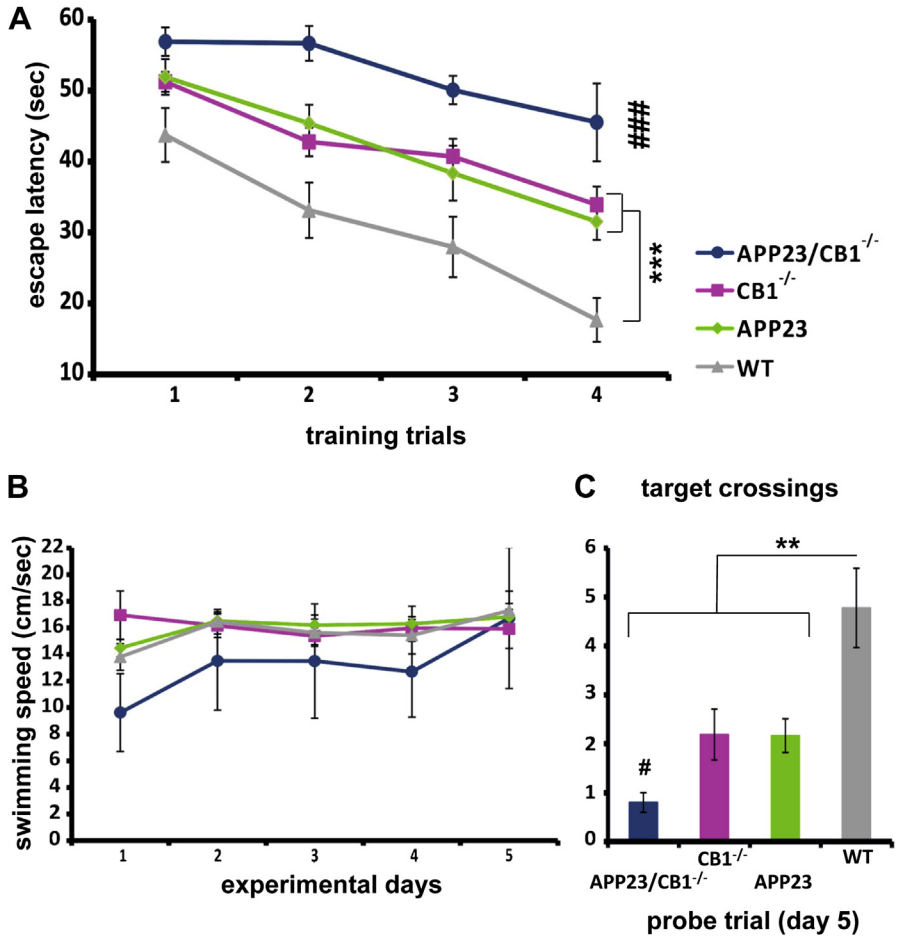

Fig. 6. Impaired cognitive performance of APP23/CB1$^{-/-}$ mice in the Morris water maze test. Escape latency during training trials (A) and the probe trail in which crossings of mice at the former platform position are counted (C). (B) Swim speed of analyzed mice is shown for training trials (days 1–4) and probe trial (day 5). Data points represent mean of 4 daily trials. Water maze data during training trials were analyzed by repeated-measures 2-way analysis of variance (Fisher least significant difference). Target crossing data during the probe trail were analyzed by Student *t* test. (***/** $p < 0.005/0.01$; ### $p < 0.005$ for APP23/CB1$^{-/-}$ compared with all other genotypes, # $p < 0.05$ for APP23/CB1$^{-/-}$ compared with all other genotypes except CB1$^{-/-}$). Abbreviations: CB1, cannabinoid receptor type 1; WT, wild type.

mice in Supplementary Fig. 3A). The reported thinning of the hippocampal CA1 region in APP23 mice compared with WT mice (Calhoun et al., 1998) was observed neither in the APP23 mice nor in APP23/CB1$^{-/-}$ mice (Fig. 5A). Overall neuronal loss in APP23/CB1$^{-/-}$ mice compared with APP23 mice was observed neither in the hippocampus nor in the neocortex. Western blot analysis to detect NeuN, a neuronal marker protein, in extracts of the hippocampus, a region that is highly sensitive to neurodegeneration, from 20-month-old mice revealed no differences among the different genotypes (Fig. 5B).

Next, possible quantitative changes in the expression of synaptic proteins were analyzed. The protein levels of synaptophysin (as presynaptic marker protein) and postsynaptic density protein 95 (PSD95) in hippocampal extracts of 20-month-old mice were similar in all genotypes as detected by Western blotting (Fig. 5B). Our data are also in line with previous results obtained from the examination of the neocortex of APP23 mice, where no differences in synaptophysin levels were observed between APP23 and WT control mice (Boncristiano et al., 2005).

3.5. Learning and memory deficits in APP23/CB1$^{-/-}$ mice

The ability to process spatial information was investigated in a standardized Morris water maze test, in which the mice were trained to localize an invisible escape platform hidden below the water surface in a large pool. Although all mice learned to find the platform after training, the escape latency (time to reach the platform) was longest for APP23/CB1$^{-/-}$ mice compared with APP23, CB1$^{-/-}$, and WT mice, strongly suggesting severe learning deficits of these mice (Fig. 6A). In addition, CB1$^{-/-}$ and APP23 mice showed learning deficits compared with WT mice but to a lower extent. APP23/CB1$^{-/-}$ mice compared with APP23 and WT mice showed also the highest and significant deficits in recalling the exact location of the platform during the probe trial, in which the platform was removed from the water tank (target crossings, Fig. 6C). The difference between APP23/CB1$^{-/-}$ and CB1$^{-/-}$ mice was not statistically significant, probably because of high variability of CB1$^{-/-}$ animals. Compared with WT mice, also APP23 and CB1$^{-/-}$ mice showed a deficit to recall the former platform location in the probe trial (Fig. 6C), consistent with previous observations made by other groups (Kelly et al., 2003; Varvel and Lichtman, 2002). Locomotor alterations of analyzed mice are not causative for the differences observed in the escape latency and target crossings because swimming speed was not significantly different among genotypes (Fig. 6B). Taken together, our data show that CB1 deficiency worsens the cognitive deficits induced by overexpressing mutant APP in the APP23 AD mouse model.

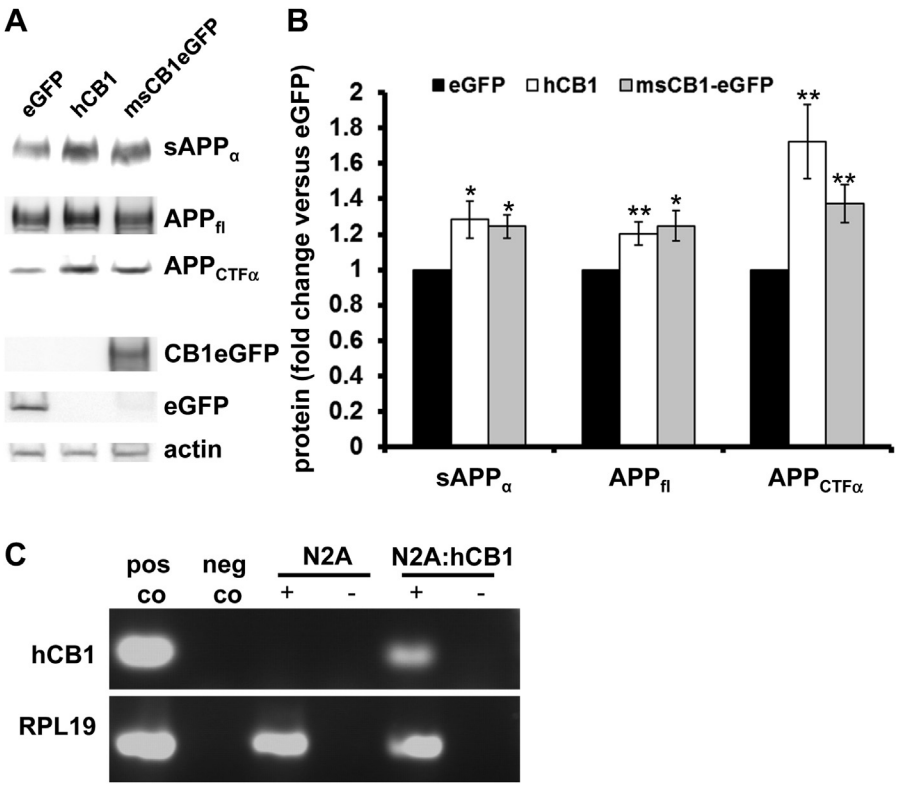

Fig. 7. CB1, cannabinoid receptor type 1 (CB1) overexpressing N2A cells show increased proteolytic amyloid precursor protein (APP) fragments. (A) Increased levels of APP full-length protein (APP_{fl}) and its proteolytic fragments resulting from α-secretase cleavage ($sAPP_{\alpha}$ and C-terminal α [CTF_{α}]) were found in N2A cells stably overexpressing human CB1 (hCB1, middle lane) or mouse CB1 coupled to eGFP (msCB1eGFP, right lane), respectively, compared with control N2A cells overexpressing solely eGFP (left lane). Data were obtained by Western blot analysis of culture supernatant (for $sAPP_{\alpha}$) or total extracts (for APP_{fl} and of CTF_{α}), respectively. (B) Data points represent mean ± standard error of the mean of 4 independent experiments for the soluble fraction and 6 independent experiments for total extracts ** $p < 0.01$, * $p < 0.05$ (Student t test). Polyclonal CB1 antibody failed to detect CB1 in N2A cells. Therefore, anti-eGFP antibody was used to detect eGFP and mouse CB1-eGFP (A). (C) Control for human CB1 overexpression in nontransfected and transfected N2A cells was performed by reverse-transcriptase polymerase chain reaction (RT-PCR). The following primers were used: hCB1 (upper panel) and ribosomal protein L19 (RPL19, lower panel, internal control). As positive controls, 2 ng hCB1 in pcDNA3 vector or an RT-PCR amplificate of RLP19 from HEK cell RNA was used, respectively. The negative control is the respective master mix without a template; "+" stands for the indicated RT-PCR reaction in nontransfected or hCB1-overexpressing N2A cells, respectively, and "–" stands for the mock controls of the RT-PCR reactions, whereas reverse transcriptase was substituted by RNAse-free water.

3.6. Levels of APP and its fragments in neuroblastoma cells with increased or reduced CB1 expression

A potential influence of CB1 expression on APP was studied in molecular detail employing in vitro cellular models. Therefore, we stably overexpressed 2 different CB1 constructs, human CB1 and mouse CB1-eGFP, respectively, in N2A neuroblastoma cells, and determined the expression of APP_{fl} and its fragments by Western blot analysis. N2A cells were chosen for these experiments because they endogenously express CB1 mRNA in contrast with other neuronal cell lines tested and thus allow manipulation of CB1 levels in both directions (up- and downregulation). CB1 overexpression in N2A cells was verified by RT-PCR for the human CB1 construct (Fig. 7C) and by Western blot using anti-eGFP antibodies for mouse CB1-eGFP (Fig. 7A). In both cell lines, the protein levels of APP_{fl}, $sAPP_{\alpha}$, and of CTF_{α} were higher than in control N2A cells that were stably transfected with the eGFP construct alone as control (APP_{fl} and CTF_{α} detected by anti-APP antibody A8717; $sAPP_{\alpha}$ detected by anti-APP antibody 22C11; Fig. 7A and B). These data support a direct link between CB1 and APP processing. The opposite experiment, a reduction of CB1 mRNA levels in N2A cells by approximately 70% after CB1 siRNA transfection (Fig. 8C), led to a significant decrease in CTF_{α} (Fig. 8A and B), again suggesting that CB1 expression and APP processing are linked. The observation that neither the APP_{fl} protein level (Fig. 8A and B) nor the APP mRNA level (Fig. 8D) was changed after CB1 siRNA transfection strongly suggests a posttranscriptional influence of CB1 on APP processing.

4. Discussion

In the present study, we describe a novel mouse model, APP23/$CB1^{-/-}$ mice, which was generated to investigate a role of CB1 in pathways and processes that are linked to AD pathogenesis. The APP23/$CB1^{-/-}$ mice showed a reduced body weight and premature death, although no obvious abnormalities regarding health status and cage behavior were detectable. In addition, we observed a significant reduction in the protein level of mutant APP, secreted sAPPα, its C-terminal α and β fragments, and $A\beta_{1-40}$ peptide in brain extracts, which coincided with a lower number of amyloid plaques and diminished glial activation in the brains of these mice. Surprisingly, the reduced number of amyloid plaques did not correlate with the cognitive parameters of the mice at all: APP23/$CB1^{-/-}$ mice displayed a reduction in amyloid plaque load and reduced inflammation in situ, but, nevertheless, these mice performed worse in the cognition tests compared with APP23 (with an intact CB1) and CB1 knockout mice. Until recently, it was suggested that the enhanced formation of Aβ and the subsequently increased amyloid plaque burden are responsible for cognitive deficits, which are the major basis of the amyloid cascade hypothesis of AD. However, mounting evidence indicates that removing amyloid

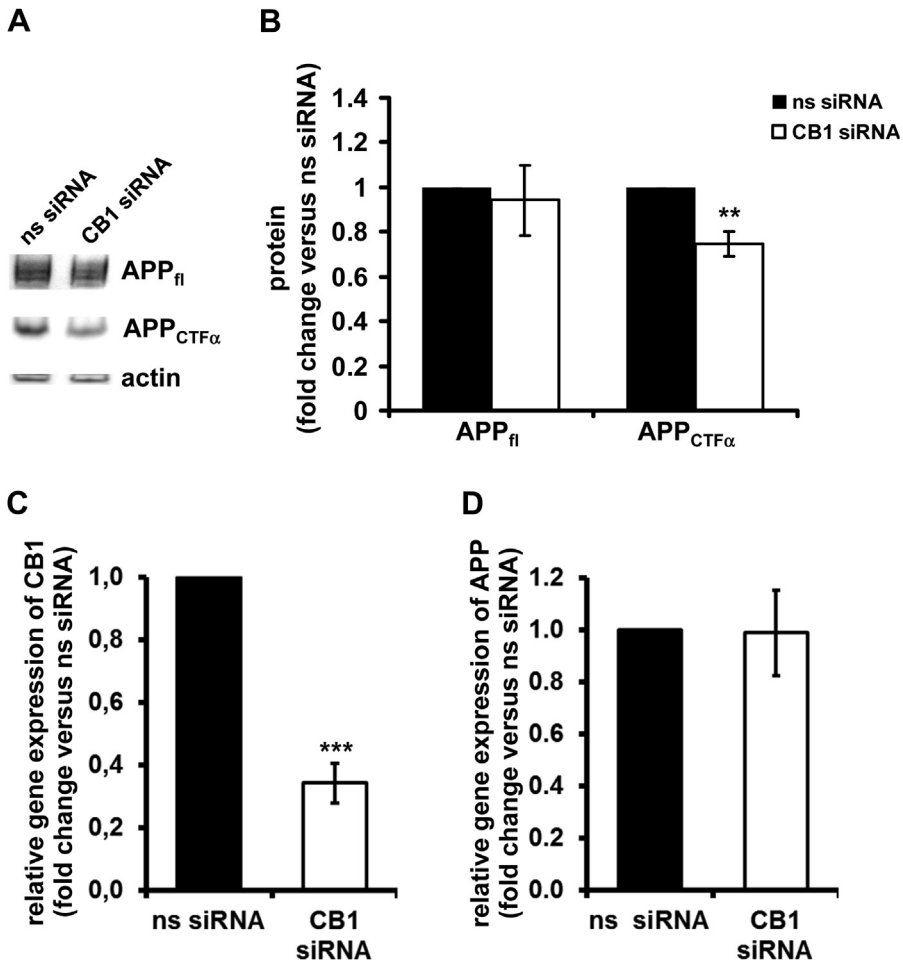

Fig. 8. Downregulation of Cannabinoid receptor type 1 (CB1) expression by transfection of N2A cells with small interfering RNA (siRNA) against mouse CB1 messenger RNA (mRNA) reduced protein levels of C-terminal α fragment (CTF_α) but not of full-length mutant APP (APP_{fl}) protein compared with N2A cells transfected with nonsense siRNA (A and B). Transcription of APP gene was not altered after CB1 siRNA treatment (D) although CB1 mRNA levels proved to be successfully reduced by nearly 70% after siRNA treatment (C) (n = 3). Shown are the means ± standard error of the mean. ** $p < 0.01$ and *** $p < 0.005$ (Student t test).

plaques does not necessarily lead to cognitive improvement and that amyloid plaques might not be the cause of AD but rather consequence of pathologic changes in brain metabolism (for review, see Williams, 2009). Interestingly, amyloid plaques are also found in the brains of individuals who had not suffered from cognitive impairment (Arriagada et al., 1992a, 1992b; Duyckaerts et al., 1998; Giannakopoulos et al., 2003; Nagy et al., 1995). Remarkably, our novel animal model, the APP23/$CB1^{-/-}$ mice, reflects to some extent the frequently observed human condition of no direct correlation of amyloid load and cognitive impairment and may help to further evaluate whether there is a link between APP and amyloid peptide formation and cognitive impairment.

In the brain sections of all mutant APP overexpressing genotypes, no overall neuronal loss could be identified by microscopical evaluation and staining with the neuronal marker NeuN, which could be directly responsible for the observed neurologic deficits. Furthermore, Western blot analysis of hippocampal extracts for pre- and postsynaptic markers (synaptophysin and PSD95) did not show a reduction in these synaptic proteins either. However, we cannot exclude that the neural networks are not functioning properly because of potential subtle changes in synaptic functions.

As stated previously, the extent of glial activation was lower in APP23/$CB1^{-/-}$ mice than in APP23 mice. Although glial activation is mainly seen as a detrimental factor, leading to pathologic neuroinflammation, neuronal dysfunction, degeneration, and ultimately to impaired memory formation (for review, see Dheen et al., 2007; Williamson et al., 2011), here, the low extent of glial activation in APP23/$CB1^{-/-}$ mice argues against a direct link of glial activation and cognitive deficits in these mice. Taken the results of the microscopical evaluation and glia-specific staining together, we speculate that very likely the significantly reduced glial activation in APP23/$CB1^{-/-}$ mice just reflects the reduced amyloid plaque load in these mice. The view that, on the other hand, the reduced glial activation in APP23/$CB1^{-/-}$ mice could be responsible for the reduced plaque load seems unlikely in light of a recent publication that states unaltered amyloid plaque formation in an AD mouse model with nearly complete loss of microglial cells (Grathwohl et al., 2009).

With respect to the premature death of a large fraction of APP23/$CB1^{-/-}$ mice, of course, the question arises whether the APP23/$CB1^{-/-}$ mice that survived into adulthood are those that became resistant to the combined detrimental effects of mutant APP overexpression and CB1 deficiency. The exact reasons why the surviving mice are resistant are so far not known and are currently under investigation. One possible explanation is that the combination of mutant APP overexpression and CB1 knockout causes an early excitotoxicity and provokes seizures, which may eventually lead to premature death in most of the APP23/$CB1^{-/-}$ animals—an

observation made in several transgenic APP mouse models (Asuni et al., 2010; Gonzalez-Tudela et al., 2011). In fact, the surviving APP23/CB1$^{-/-}$ animals might be more resistant to seizures. Whether the observed changes in APP processing affect survival of APP23/CB1$^{-/-}$ animals remains to be analyzed.

To further investigate direct consequences of altered CB1 expression on APP processing in APP23/CB1$^{-/-}$, we established a cellular in vitro system. We stably overexpressed CB1 in N2A cells and could indeed confirm an influence of altered CB1 expression on APP processing. We found that increased CB1 expression in this neuronal cell line led to increased levels of APP_{fl} protein and an increased amount of APP fragments. Consistently, reduced CB1 expression as reached by transfection of N2A cells with CB1 siRNA led to a reduced production of APP fragments, although the amount of APP_{fl} protein was unchanged. Therefore, we confirmed in vitro, at least in part, the results on the effect of CB1 deficiency on APP processing obtained in APP23/CB1$^{-/-}$ mice. Taken together, our in vivo and the in vitro data support a molecular link between CB1 expression and APP processing.

How CB1 exactly affects APP processing and whether CB1 and APP are directly or indirectly linked needs to be further investigated. The altered processing of APP, which results in a reduced amount of APP-cleavage fragments and, in consequence, also in a reduced number of amyloid plaques in APP23/CB1$^{-/-}$ mice, may also be because of changes in intracellular APP transport. An influence of various G protein–coupled receptors on APP processing has been already described. Stimulation of the muscarinic acetylcholine receptor M1 has been shown to promote anti-amyloidogenic processing of APP by an unknown mechanism, and knockout of this receptor led to an increase in amyloid plaque number in an AD mouse model (Davis et al., 2010). Teng et al. (2010) have shown that the δ-opioid receptor forms a complex with β- and γ-secretase and thus promotes the processing of APP to Aβ peptides by these enzymes. Interestingly, this interaction seems to specifically affect APP processing but not the processing of other γ-secretase substrates such as Notch, cadherin, and the APP-like protein (APLP). Thathiah et al. (2009) identified the G protein–coupled receptor 3 (GPR3), a constitutively active orphan G protein–coupled receptor, as a modulator of toxic Aβ peptide production. Here, the mechanism by which the G protein–coupled receptor affects APP processing has been described to involve increased γ-secretase complex formation and translocation of the mature complex to the plasma membrane, where it is preferentially incorporated in detergent-resistant membrane fractions. GPR3 activity results in increased processing of APP to Aβ peptides, whereas GPR3 knockout in an AD mouse model leads to reduced Aβ peptide levels. Similar to the δ-opioid receptor, GPR3 does not affect Notch processing. Collectively, all these studies report a modulation of APP processing by different G protein–coupled receptors. Whether CB1 and APP, both transmembrane proteins, even interact physically also needs to be investigated. Taken together, the details of the underlying exact molecular mechanisms of the CB1-APP interaction remain an open question which we will attempt to address for the CB1 receptor in further studies using the newly generated, CB1 stably overexpressing N2A cells and our APP23/CB1$^{-/-}$ animal model. Moreover, this particular CB1-deficiency mouse model in APP23 background showing memory impairment but a lower amyloid plaque load will be useful for future investigations of the role of APP and Aβ peptides in AD.

Acknowledgements

The authors would like to thank U. Schmitt (Department of Psychiatry, Mainz) for invaluable help with water maze experiments, J. Trotter for anti-PSD95 antibody, A. Bilkei-Gorzo for help with statistics, M. Staufenbiel (Novartis, Basel) for providing APP23 mice, and C. Ziegler for helpful comments on the manuscript. This work was performed in the framework of the DFG research group (DFG FOR 926; grants to CB and BL) and the DFG CRC 1080 (grant to CB).

Appendix A. Supplementary data

Supplementary data associated with this article can be found, in the online version, at http://dx.doi.org/10.1016/j.neurobiolaging.2013.05.027.

References

Arriagada, P.V., Growdon, J.H., Hedley-Whyte, E.T., Hyman, B.T., 1992a. Neurofibrillary tangles but not senile plaques parallel duration and severity of Alzheimer's disease. Neurology 42 (Pt 1), 631–639.

Arriagada, P.V., Marzloff, K., Hyman, B.T., 1992b. Distribution of Alzheimer-type pathologic changes in nondemented elderly individuals matches the pattern in Alzheimer's disease. Neurology 42, 1681–1688.

Aso, E., Palomer, E., Juves, S., Maldonado, R., Munoz, F.J., Ferrer, I., 2012. CB1 agonist ACEA protects neurons and reduces the cognitive impairment of AbetaPP/PS1 mice. J. Alzheimers Dis. 30, 439–459.

Asuni, A.A., Perry, V.H., O'Connor, V., 2010. Change in tau phosphorylation associated with neurodegeneration in the ME7 model of prion disease. Biochem. Soc. Trans. 38, 545–551.

Benard, G., Massa, F., Puente, N., Lourenco, J., Bellocchio, L., Soria-Gomez, E., Matias, I., Delamarre, A., Metna-Laurent, M., Cannich, A., Hebert-Chatelain, E., Mulle, C., Ortega-Gutierrez, S., Martin-Fontecha, M., Klugmann, M., Guggenhuber, S., Lutz, B., Gertsch, J., Chaouloff, F., Lopez-Rodriguez, M.L., Grandes, P., Rossignol, R., Marsicano, G., 2012. Mitochondrial CB(1) receptors regulate neuronal energy metabolism. Nat. Neurosci. 15, 558–564.

Benito, C., Nunez, E., Tolon, R.M., Carrier, E.J., Rabano, A., Hillard, C.J., Romero, J., 2003. Cannabinoid CB2 receptors and fatty acid amide hydrolase are selectively overexpressed in neuritic plaque-associated glia in Alzheimer's disease brains. J. Neurosci. 23, 11136–11141.

Bisogno, T., Di Marzo, V., 2008. The role of the endocannabinoid system in Alzheimer's disease: facts and hypotheses. Curr. Pharm. Des. 14, 2299–3305.

Boncristiano, S., Calhoun, M.E., Howard, V., Bondolfi, L., Kaeser, S.A., Wiederhold, K.H., Staufenbiel, M., Jucker, M., 2005. Neocortical synaptic bouton number is maintained despite robust amyloid deposition in APP23 transgenic mice. Neurobiol. Aging 26, 607–613.

Brahmachari, S., Fung, Y.K., Pahan, K., 2006. Induction of glial fibrillary acidic protein expression in astrocytes by nitric oxide. J. Neurosci. 26, 4930–4939.

Buchser, W.J., Pardinas, J.R., Shi, Y., Bixby, J.L., Lemmon, V.P., 2006. 96-Well electroporation method for transfection of mammalian central neurons. Biotechniques 41, 619–624.

Calhoun, M.E., Wiederhold, K.H., Abramowski, D., Phinney, A.L., Probst, A., Sturchler-Pierrat, C., Staufenbiel, M., Sommer, B., Jucker, M., 1998. Neuron loss in APP transgenic mice. Nature 395, 755–756.

Chen, X., Zhang, J., Chen, C., 2011. Endocannabinoid 2-arachidonoylglycerol protects neurons against beta-amyloid insults. Neuroscience 178, 159–168.

Cota, D., Marsicano, G., Tschop, M., Grubler, Y., Flachskamm, C., Schubert, M., Auer, D., Yassouridis, A., Thone-Reineke, C., Ortmann, S., Tomassoni, F., Cervino, C., Nisoli, E., Linthorst, A.C., Pasquali, R., Lutz, B., Stalla, G.K., Pagotto, U., 2003. The endogenous cannabinoid system affects energy balance via central orexigenic drive and peripheral lipogenesis. J. Clin. Invest. 112, 423–431.

Davis, A.A., Fritz, J.J., Wess, J., Lah, J.J., Levey, A.I., 2010. Deletion of M1 muscarinic acetylcholine receptors increases amyloid pathology in vitro and in vivo. J. Neurosci. 30, 4190–4196.

Dheen, S.T., Kaur, C., Ling, E.A., 2007. Microglial activation and its implications in the brain diseases. Curr. Med. Chem. 14, 1189–1197.

Dodd, G.T., Mancini, G., Lutz, B., Luckman, S.M., 2010. The peptide hemopressin acts through CB1 cannabinoid receptors to reduce food intake in rats and mice. J. Neurosci. 30, 7369–7376.

Duyckaerts, C., Colle, M.A., Dessi, F., Piette, F., Hauw, J.J., 1998. Progression of Alzheimer histopathological changes. Acta Neurol. Belg. 98, 180–185.

Esposito, G., Scuderi, C., Valenza, M., Togna, G.I., Latina, V., De Filippis, D., Cipriano, M., Carratu, M.R., Iuvone, T., Steardo, L., 2011. Cannabidiol reduces Abeta-induced neuroinflammation and promotes hippocampal neurogenesis through PPARgamma involvement. PloS One 6, e28668.

Eubanks, L.M., Rogers, C.J., Beuscher, A.E., Koob, G.F., Olson, A.J., Dickerson, T.J., Janda, K.D., 2006. A molecular link between the active component of marijuana and Alzheimer's disease pathology. Mol. Pharm. 3, 773–777.

Fakhfouri, G., Ahmadiani, A., Rahimian, R., Grolla, A.A., Moradi, F., Haeri, A., 2012. Win55212-2 attenuates amyloid-beta-induced neuroinflammation in rats through activation of cannabinoid receptors and PPAR-gamma pathway. Neuropharmacology 63, 653–666.

Giannakopoulos, P., Herrmann, F.R., Bussiere, T., Bouras, C., Kovari, E., Perl, D.P., Morrison, J.H., Gold, G., Hof, P.R., 2003. Tangle and neuron numbers, but not

amyloid load, predict cognitive status in Alzheimer's disease. Neurology 60, 1495–1500.
Gonzalez-Tudela, A., Martin-Cano, D., Moreno, E., Martin-Moreno, L., Tejedor, C., Garcia-Vidal, F.J., 2011. Entanglement of two qubits mediated by one-dimensional plasmonic waveguides. Phys. Rev. Lett. 106, 020501.
Grathwohl, S.A., Kalin, R.E., Bolmont, T., Prokop, S., Winkelmann, G., Kaeser, S.A., Odenthal, J., Radde, R., Eldh, T., Gandy, S., Aguzzi, A., Staufenbiel, M., Mathews, P.M., Wolburg, H., Heppner, F.L., Jucker, M., 2009. Formation and maintenance of Alzheimer's disease beta-amyloid plaques in the absence of microglia. Nat. Neurosci. 12, 1361–1363.
Haass, C., Selkoe, D.J., 2007. Soluble protein oligomers in neurodegeneration: lessons from the Alzheimer's amyloid beta-peptide. Nat. Rev. Mol. Cell Biol. 8, 101–112.
Huang, Y., Mucke, L., 2012. Alzheimer mechanisms and therapeutic strategies. Cell 148, 1204–1222.
Iuvone, T., Esposito, G., De Filippis, D., Scuderi, C., Steardo, L., 2009. Cannabidiol: a promising drug for neurodegenerative disorders? CNS Neurosci. Ther. 15, 65–75.
Johnston, H., Boutin, H., Allan, S.M., 2011. Assessing the contribution of inflammation in models of Alzheimer's disease. Biochem. Soc. Trans. 39, 886–890.
Jung, K.M., Astarita, G., Yasar, S., Vasilevko, V., Cribbs, D.H., Head, E., Cotman, C.W., Piomelli, D., 2012. An amyloid beta42-dependent deficit in anandamide mobilization is associated with cognitive dysfunction in Alzheimer's disease. Neurobiol. Aging 33, 1522–1532.
Karl, T., Cheng, D., Garner, B., Arnold, J.C., 2012. The therapeutic potential of the endocannabinoid system for Alzheimer's disease. Expert Opin. Ther. Targets 16, 407–420.
Kelly, P.H., Bondolfi, L., Hunziker, D., Schlecht, H.P., Carver, K., Maguire, E., Abramowski, D., Wiederhold, K.H., Sturchler-Pierrat, C., Jucker, M., Bergmann, R., Staufenbiel, M., Sommer, B., 2003. Progressive age-related impairment of cognitive behavior in APP23 transgenic mice. Neurobiol. Aging 24, 365–378.
Lalonde, R., Dumont, M., Staufenbiel, M., Strazielle, C., 2005. Neurobehavioral characterization of APP23 transgenic mice with the SHIRPA primary screen. Behav. Brain Res. 157, 91–98.
Marsicano, G., Moosmann, B., Hermann, H., Lutz, B., Behl, C., 2002a. Neuroprotective properties of cannabinoids against oxidative stress: role of the cannabinoid receptor CB1. J. Neurochem. 80, 448–456.
Marsicano, G., Wotjak, C.T., Azad, S.C., Bisogno, T., Rammes, G., Cascio, M.G., Hermann, H., Tang, J., Hofmann, C., Zieglgansberger, W., Di Marzo, V., Lutz, B., 2002b. The endogenous cannabinoid system controls extinction of aversive memories. Nature 418, 530–534.
Martin-Moreno, A.M., Brera, B., Spuch, C., Carro, E., Garcia-Garcia, L., Delgado, M., Pozo, M.A., Innamorato, N.G., Cuadrado, A., Ceballos, M.L., 2012. Prolonged oral cannabinoid administration prevents neuroinflammation, lowers beta-amyloid levels and improves cognitive performance in Tg APP 2576 mice. J. Neuroinflammation 9, 8.
Martin-Moreno, A.M., Reigada, D., Ramirez, B.G., Mechoulam, R., Innamorato, N., Cuadrado, A., de Ceballos, M.L., 2011. Cannabidiol and other cannabinoids reduce microglial activation in vitro and in vivo: relevance to Alzheimer's disease. Mol. Pharmacol. 79, 964–973.
Mazzola, C., Micale, V., Drago, F., 2003. Amnesia induced by beta-amyloid fragments is counteracted by cannabinoid CB1 receptor blockade. Eur. J. Pharmacol. 477, 219–225.
Milton, N.G., 2002. Anandamide and noladin ether prevent neurotoxicity of the human amyloid-beta peptide. Neurosci. Lett. 332, 127–130.
Morris, R.G., Garrud, P., Rawlins, J.N., O'Keefe, J., 1982. Place navigation impaired in rats with hippocampal lesions. Nature 297, 681–683.
Mulder, J., Zilberter, M., Pasquare, S.J., Alpar, A., Schulte, G., Ferreira, S.G., Kofalvi, A., Martin-Moreno, A.M., Keimpema, E., Tanila, H., Watanabe, M., Mackie, K., Hortobagyi, T., de Ceballos, M.L., Harkany, T., 2011. Molecular reorganization of endocannabinoid signalling in Alzheimer's disease. Brain 134 (Pt 4), 1041–1060.
Nagy, Z., Esiri, M.M., Jobst, K.A., Morris, J.H., King, E.M., McDonald, B., Litchfield, S., Smith, A., Barnetson, L., Smith, A.D., 1995. Relative roles of plaques and tangles in the dementia of Alzheimer's disease: correlations using three sets of neuropathological criteria. Dementia 6, 21–31.
Persson, A., Osman, A., Bolouri, H., Mallard, C., Kuhn, H.G., 2013. Radixin expression in microglia after cortical stroke lesion. Glia 61, 790–799.
Pfaffl, M.W., Horgan, G.W., Dempfle, L., 2002. Relative expression software tool (REST) for group-wise comparison and statistical analysis of relative expression results in real-time PCR. Nucleic Acids Res. 30, e36.
Postina, R., Schroeder, A., Dewachter, I., Bohl, J., Schmitt, U., Kojro, E., Prinzen, C., Endres, K., Hiemke, C., Blessing, M., Flamez, P., Dequenne, A., Godaux, E., van Leuven, F., Fahrenholz, F., 2004. A disintegrin-metalloproteinase prevents amyloid plaque formation and hippocampal defects in an Alzheimer disease mouse model. J. Clin. Invest. 113, 1456–1464.
Ramirez, B.G., Blazquez, C., Gomez del Pulgar, T., Guzman, M., de Ceballos, M.L., 2005. Prevention of Alzheimer's disease pathology by cannabinoids: neuroprotection mediated by blockade of microglial activation. J. Neurosci. 25, 1904–1913.
Schellenberg, G.D., Montine, T.J., 2012. The genetics and neuropathology of Alzheimer's disease. Acta Neuropathol. 124, 305–323.
Schmitt, U., Hiemke, C., Fahrenholz, F., Schroeder, A., 2006. Over-expression of two different forms of the alpha-secretase ADAM10 affects learning and memory in mice. Behav. Brain Res. 175, 278–284.
Sturchler-Pierrat, C., Abramowski, D., Duke, M., Wiederhold, K.H., Mistl, C., Rothacher, S., Ledermann, B., Burki, K., Frey, P., Paganetti, P.A., Waridel, C., Calhoun, M.E., Jucker, M., Probst, A., Staufenbiel, M., Sommer, B., 1997. Two amyloid precursor protein transgenic mouse models with Alzheimer disease-like pathology. Proc. Natl Acad. Sci. U.S.A. 94, 13287–13292.
Teng, L., Zhao, J., Wang, F., Ma, L., Pei, G., 2010. A GPCR/secretase complex regulates beta- and gamma-secretase specificity for Abeta production and contributes to AD pathogenesis. Cell. Res. 20, 138–153.
Thathiah, A., Spittaels, K., Hoffmann, M., Staes, M., Cohen, A., Horre, K., Vanbrabant, M., Coun, F., Baekelandt, V., Delacourte, A., Fischer, D.F., Pollet, D., De Strooper, B., Merchiers, P., 2009. The orphan G protein-coupled receptor 3 modulates amyloid-beta peptide generation in neurons. Science 323, 946–951.
van der Stelt, M., Mazzola, C., Esposito, G., Matias, I., Petrosino, S., De Filippis, D., Micale, V., Steardo, L., Drago, F., Iuvone, T., Di Marzo, V., 2006. Endocannabinoids and beta-amyloid-induced neurotoxicity in vivo: effect of pharmacological elevation of endocannabinoid levels. Cell. Mol. Life Sci. 63, 1410–1424.
Varvel, S.A., Lichtman, A.H., 2002. Evaluation of CB1 receptor knockout mice in the Morris water maze. J. Pharmacol. Exp. Ther. 301, 915–924.
Williams, M., 2009. Progress in Alzheimer's disease drug discovery: an update. Curr. Opin. Investig. Drugs 10, 23–34.
Williamson, L.L., Sholar, P.W., Mistry, R.S., Smith, S.H., Bilbo, S.D., 2011. Microglia and memory: modulation by early-life infection. J. Neurosci. 31, 15511–15521.